Characteristics of Erosion Development and Dynamics of Gravelly Debris Flow in The Houyenshan of Taiwan

Yu-Sen Lai
National Yang Ming Chiao Tung University
Chia-Ming Lo (cmlo@nctu.edu.tw)
National Yang Ming Chiao Tung University
Meng-Chia Weng
National Yang Ming Chiao Tung University
Yen-Hsin Chung
National United University

Research Article

Keywords: erosion development, gravelly debris flow, geomorphology interpretation, field investigation, discrete element method

Posted Date: May 4th, 2021

DOI: https://doi.org/10.21203/rs.3.rs-455305/v1

Abstract

This study focused on the erosion development and dynamics of gravelly debris flow at the Houyenshan watershed through geomorphology interpretation, field investigation, and discrete element method. The study constructed a discrete element method to simulate the process of gravelly debris flow and determine the scope of influence with regard to deposition. And then, the study integration of the interpretation, field investigation, and simulation results to evaluate erosion and landslide hazard in study area. Finally, the results can serve as a reference for disaster prevention, mapping and zoning of the areas susceptible to geological hazards, and associated mitigation project planning.

1. Introduction

From east to west, the Houyenshan area of Miaoli County, Taiwan encompasses five pits (Fig. 1). According to geological map (Fig. 2), the area includes the Toukoshan Formation and a sedimentary layer of red soil. The Toukoshan Formation is further divided into the Xiangshan phase and the Houyenshan phase and belongs to the Pleistocene epoch of the Quaternary period. The Houyenshan phase is mainly a thick layer of gravel interlaced with sandstone and red soil. The strong rainfall brought by typhoons erodes the surface of the gravel layer and increases surface runoff, which can easily erode and scour the fine particulate matter cementing the gravel, thereby promoting the development of erosion gullies.

The prevalence of erosion gullies in Houyenshan is the result of rainfall as well as the terrain conditions. Yo et al. (2005) observed that the slope collapses and debris flows in this area all took place on converged convex slopes, which indicate that such terrain is conducive to the pooling of runoff from above and leads to surface erosion. At the same time, convex slopes provide collapsed masses with steeper and thus better environments for sliding, which result in short-distance debris flows. Chou (2013) compared field investigation results and LIDAR scans and found that the mechanisms of debris flows in Houyenshan to be guided by scarp deposits in the source area upstream and the destruction of or overflow over earthworks on streambeds. Based on spectrum analysis results, Chou et al. (2015) discovered that surface runoff and debris flows have better geophone and acoustic signal responses and that the main frequency distributions on surface runoff spectra are slightly higher than those of debris flow spectra. Furthermore, rainfall scale and source material deposits determine the patterns and range of debris flows. Lin et al. (2007) observed two types of slope retreat in Houyenshan: parallel slope retreat, which generally occurs in places with greater transportation capacity, and slope reduction, which mostly takes place on cataclinal slopes. In the source area of Catchment No. 3, reduction rates reached 3 meters every year. Lin et al. (2008) simulated the streambed transport patterns of gravel in an experiment tank. On a gentle streambed (less than 4°), the transport quantity of the bed load is not very high, but during torrential rains when the river flow is greater than 2 m/sec, the gravel can be transported easily. This indicates that the gravel transport capability of water with high flow rates is very strong. In contrast, gravel can be moved from its original location very easily on river beds with a slope greater than 7° (15%) if there are no particular obstacles. Lin (2009) indicated that if the rain is not heavy, generally only Catchment No. 3 has any responses. During significant rainfall events, responses appear in all of the

catchments. Furthermore, rainfall greater than 100 mm within 12 hours generally leads to gravelly debris flows.

This study integrated the research above and survey data and used numerical simulation to simulate the transport processes in landslide areas from 2008 to 2016. With high-precision aerial surveys and field investigations, we used numerical simulation and interpreted historical images to assess the potential landslide hazard in the study area.

2. Methodology

This study included the interpretation of terrain data that was collected and remote sensing images from different periods of time, field investigations, and PFC3D numerical simulations.

2.1 Terrain analysis method and remote sensing image interpretation

With contour lines as the basis for analysis, historical topographic maps show that denser contour lines indicate greater variations in height and steep cliffs. A simple way of determining whether a location is susceptible to landslides is the presence of inverse and gentler contour lines in the middle of dense contour lines, which indicate hummocky terrain. The topographic map roughly shows that the study area has a valley terrain featuring concave slopes (the tips of the V-shaped contour lines pointing upwards). The contour lines on both sides of the streams are of equal height because the slopes are steep and easily eroded by rain. We overlaid remote sensing images from different years one over another to compare and understand the landslide conditions of each year and mark the sliding masses. From the images, we could detect five gravel deposits on the alluvial plain. Following field investigation, we referred to the slope stability classification (Table 1) proposed by Crozer in 1984 to determine the stability of potential sliding masses.

Table 1
Landslide activity classification

(modified from Crozier 1984)

CLASS	DESCRIPTION
Unstable Slopes	
I_a	Active landslides; material is currently moving, and landslide features are fresh and well defined
I_b	Reactivated landslide; material is currently moving and represents renewed landslide activity; some landslide features are fresh and well defined; others may appear older.
I_c	Suspended landslides; slopes with evidence of landslide activity within the past year; landslide features are fresh and well defined.
Slopes With Inactive Landslides	
II_a	Dormant-historic landslides; slopes with evidence of previous landslide activity that have undergone most recent movement within the preceding 10 years.
II_b	Dormant-young landslides; slopes with evidence of previous landslide activity that have undergone most recent movement within the preceding 10 to 50 years.
II_c	Dormant-mature landslides; slopes with evidence of previous landslide activity that have undergone most recent movement within the preceding 50 to 100 years.
II_d	Dormant-old landslides; slopes with evidence of previous landslide activity that have undergone most recent movement more than 100 years.
III Potentially Unstable Slopes	
	Slope that no evidence of previous landslide activity but that are considered likely to develop landslides in the future; landslide potential is indicated by analysis or comparison with other slopes.

2.2 Field investigation

We used an unmanned aerial vehicle (UAV) for photogrammetry and outcrop investigation. Image processing was performed using the PhotoScan photogrammetry software developed by AgiSoft to create three-dimensional models. This enabled us to look at the landslide conditions in each area with minimal investigation time. This software program can create digital elevation models (DEMs) and high-precision aerial photos for ArcGis analysis and numerical simulations.

2.3 Numerical simulation

(1) We used PFC3D, which was established based on the discrete element method. PFC is a discrete element analysis program developed by Itasca in 1999 (Itasca, 2002) and mainly uses the explicit finite difference method to calculate changes in the system at each time step. For each time step, the locations of the particles and the amount of overlapping are first calculated. Contact forces are then calculated

based on the force-displacement law, following which the new particle speeds and locations can be derived using Newton's second law of motion.

(2) Ball establishment first requires the relationship between landslide area and depth. The relative elevation locations of the digital terrain in the latest year (post-landslide terrain) are subtracted from the digital terrain of the previous year (pre-landslide terrain) to determine the relationship between landslide area and depth (Fig. 3). As landslide depth may vary, 20 measurement points were adopted for each sliding mass to calculate the mean landslide depth for reference in ball element simulation depth.

(3) The files for the generated wall and ball elements in a 5×5m DEM were too large for a computer to bear. As a result, we converted the 5×5m DEM into a 10×10m DEM and established 52,392 wall elements in the irregular terrain. We experimented on 5,380 and 7,380 ball elements to simulate the movements of historical landslides in 2008 and 2016. The parameter settings in this study were based on physical test results and relationships between macroscopic and microscopic parameters established by Chang et al. (2014) using multiple regression analysis. Simulation tests indicated that ball element radii between 2.5 m and 5 m resulted in the best computation performance and deposits most similar to those found onsite (Lo, 2016). Smaller radii would have produced even greater similarity, but considering the issue of time and possible damage to the computer equipment, we did not adopt radii smaller than 2.5 m for the ball elements. Table 2 presents the relevant simulation parameters.

Table 2
The numerical parameters of the PFC modeling in this study

Parameter	Full-scale model parameter
Unit weight of ball elements (kg/m^3)	2,350
Distribution of ball element radii (m)	2.5
Normal stiffness (kN/m)	5.6e8
Shear stiffness (kN/m)	5.6e8
Friction coefficients of ball elements	0.25–0.5
Friction coefficient of wall elements	0.6
Normal stiffness of parallel bonds (kN/m^3)	4e8-4.3e8
Shear stiffness of parallel bonds (kN/m^3)	2e8-2.1e8
Normal strength of parallel bonds (Mpa)	15–17
Shear strength of parallel bonds (Mpa)	7–8
Normal damping coefficient	0.32–0.4
Shear damping coefficient	0.05–0.2

3. Results

3.1 Terrain analysis method and remote sensing image interpretation

(a) The analysis results in Fig. 4 show the influence of long-term erosion in the study area in 1920. Distinct hummocky surfaces could be seen near Pit No. 3 in 1992; any typhoon or earthquake would have accelerated the damage of the hummocky surfaces. By 1999, the hummocky surfaces had already been damaged. The landslide scope increased substantially in a short seven years. Aside from the hummocky surfaces accelerating terrain changes, the geological environmental also meant that slope surfaces were easily eroded by rain, thereby preventing vegetation growth.

(b) In the remote sensing images from 2008 and 2016 (Fig. 5), the image from 2008 revealed that the five pits were continuously expanding towards the north and to the sides. Among the deposits on the alluvium plains below, that of Pit No. 3 contained the most sand. Pit No. 3 presented the most significant changes in the remote sensing image from 2016; it expanded outwards on all sides. The landslide area of Pit No. 5 showed some no vegetation growing. Larger landslides mostly took place in the source area.

(C) Fig. 6 displays the changes in the five pits from 2005 to 2015 in five small images, which were then divided into masses by area and marked by the year that they collapsed. These show that the sliding masses continued to move throughout the years, which can enable the zoning for historical landslides in the numerical simulations.

3.2 Field investigation

(a) Statistics from 2002 to 2008 (Fig. 7) indicate that the erosion rates in Sect. 3 − 1 and 3 − 2 were both greater than 10. In contrast, the erosion rates in the other sections were less than 3. The statistics from 2008 to 2016 displayed lower erosion rates and the approach of stability. The cliff lines of Pit No. 4 in the remote sensing images from the three years showed less significant slope retreat in Pit No. 4. The most significant cause of varying degrees of erosion was the uneven distribution of erosion gully development. In the study area, the erosion gullies in Pit No. 3 were the most severe.,

(b) Based on the field investigation, the landslide mechanisms in the source area could be divided into five stages. In the first stage before rainfall, the gravel and fine particles reach equilibrium, which promote slope stability. In the second stage, when rain begins to fall and the surface runoff increases, the gravel becomes wet due to its high porosity. In the third stage, continuous rainfall leads to the continuous scour and loss of fine surface particles, which do not immediately fall into the stream but are deposited at the slope toe. The larger gravel remaining on the surface support one another, and the slope begins to lose stability. In the fourth state, the rainfall increases, leading to the excessive loss of fine particles and the gradual formation of the sliding face. Due to rising pore pressure and reduced shear strength in the gravel

slope, the gravel layer begins to slide. In the fifth stage, after the landslide, tension cracks form at the top of the gravel slope, and the cycle repeats.

(C) In potential landslide stability classification (Fig. 8), the slope stability classification proposed by Crozer (1984) indicates that the study area belongs to Class I, unstable slopes. There is evidence of significant changes in recent years. Ia indicates highly active landslide slopes on which the landslide materials are still sliding at a total of 17 places. Ten of these places are in Pit No. 10, where the hazardous sliding masses are all at the source. Ib marks the landslide materials that are still sliding, with six places showing signs of sliding further. Ic are the slopes on which landslides have taken place in recent years. These slopes show evidence of landslides occurring in recent years at 11 places.

3.3 Numerical simulation of landslides

The grey region marks the study area, and the red balls are the historical landslide areas. Having the high-precision aerial photos from 2008 and 2016, we could perform simulations and compare the results with the onsite conditions. Images from Formosat-2 for 10 years provided more information for verification. Figure 9 shows the simulation of the historical landslide processes in 2008. The simulation results were as follows:

(a) With ball element radius set at 2.5 m and 5,380 ball elements in total, the depth of the historical landslide in Pit No. 1 ranged from 9 m to 13 m. The ball elements were arranged in three layers. The depth of the historical landslide in Pit No. 2 ranged from 8 m to 11 m, the ball elements also arranged in three layers. The maximum depth of the historical landslide in Pit No. 3 reached 26 m, and the ball elements were arranged in six layers. The depth of the historical landslide in Pit No. 4 was approximately 7 m, and the ball elements were arranged in two layers. The depth of the historical landslide in Pit No. 5 was roughly 12 m, and the ball elements were arranged in three layers.

(b) At Step 9,400, the sliding speed in Pit No. 5 was higher than those in the other four pits. The river channel in Pit No. 5 is straighter than those in the other four pits, and the source area was the lowest in elevation. At Step 294,000, most of the sliding mass in Pit No. 3 in the image had already been deposited in the stream, while those in the other pits were gradually being deposited at the river mouth. At Step 774,070, the gravel in Pit No. 3 was moving more slowly in the middle section of the river channel, which was bent slightly and somewhat obstructed the rolling of the gravel. At Step 1,254,070, the majority of the gravel had left the river channel and entered the alluvial fan below.

(c) The gravel transport and alluvial fan deposits in the remote sensing images from 2008 and 2007 were similar to those in the numerical simulation at Step 554,070, which indicate no significant errors in the parameter settings. The debris washed down in Fig. 9 did not pile upwards but moved towards the sides. Only when the debris encountered obstacles in the terrain did is continue to pile upwards. The transport conditions in Pits No. 1 and 5 in the numerical simulations showed that without disaster prevention measures, typhoons would bring down substantial amounts of debris, thereby burying the tunnel exits.

The tunnel also had to bear the weight of the debris washed down in Pit No. 3, which means that regular tunnel checks are needed to preserve the safety of road users. Figure 10 displays the simulation results of the historical landslide processes prior to 2016:

(d) With ball element radius set at 2.5 m and 7,380 ball elements in total, the layer arrangements in Pits No. 1 through 5 were the same as those for the 2008 simulation. At Step 0, the ball elements at the top in Pit No. 3 had already passed the ridgeline. The landslide area was greater than that in 2008, while the remaining landslide areas were mainly in the source areas of the respective pits.

(e) As the landslide area had already passed the ridgeline, some of the ball elements in the source area of Pit No. 3 fell off the sides at Step 194,050. The remainder of the sliding mass fell in the river channel. At Step 674,051, the alluvial fan gradually formed. Observation revealed that the deposits on the alluvial fan in Pit No. 3 at Step 674,050 were different from those in the 2008 simulation. Originally, the deposits continuously extended to the sides and rarely piled upwards. However, in this simulation, the deposits piled upwards, possibly due to the larger landslide area in Pit No. 3 as well as the significantly larger landslide area on both sides of the river channel at the middle section. This resulted in debris being washed down from the source area after the landslide in the middle section, which caused a substantial amount of debris being moved to the alluvial fan at once.

(f) A comparison of the numerical simulation with the remote sensing image of 2016 revealed that most of the alluvial fan had been covered in vegetation by 2015. The deposits on the left of river mouth No. 3 were higher than those on the right. The debris scoured down moved downwards. In 2016, river mouth No. 3 showed signs of debris flow movement, and once the alluvial fan deposits above the tunnel reached a certain height, they extended towards the riverbed.

4. Landslide Risk Zoning And Hazard Classification

We mainly referred to a Swiss hazard classification and integrated the results of this study and previous experience for zoning. Furthermore, we used the results of the PFC3D numerical simulations and field investigations to create the landslide hazard map. According to the frequency and location of landslide occurrence in the different areas, we formulated a criteria table for landslide hazard map application (Table 3).

Table 3
Criteria table for application of landslide hazard map of study area

Class of landslide hazard	Application criteria of landslide hazard class
High hazard (High hazard)	These areas include source areas and areas of high landslide frequency. Hiking and development are prohibited, so in the event of a landslide, the landslide area at the source area expands at once. Typhoons and torrential rains can cause hiking paths and entrances to change at any time.
Medium hazard (Medium hazard)	These areas include areas near scarps and are the main focuses of remediation and monitoring. The protected target is the tunnel, which may suffer severe damage. Furthermore, the exits to the east and west may be burying by debris flows, so access should be prohibited during typhoons.
Low hazard (Low hazard)	These areas include the tunnel and outer edges of the alluvial fans. The protected targets include structures outside of the tunnel and buildings, which may suffer a small amount of damage. In the event that road works, evacuation routes, and shelters must be established within these areas, the structure types and internal shelter configurations must be taken into consideration.
Very low hazard (Very low hazard)	Warning signs should be erected in these areas. In the event of landslide disasters and continuous rainfall over multiple days, people should avoid taking part in activities in these areas.

5. Conclusion

This study combined landslide microfeatures, geomorphological interpretations, and PFC3D numerical simulations to simulate landslide disasters in the catchment area of the Houyenshan Nature Reserve. In addition to high-precision photogrammetry abd field investigations, we collected historical remote sensing images to interpret the locations of landslide disasters in the catchment area and established the relationship between landslide area and depth to investigate gravel erosion development and transport characteristics. Field investigations of the landslide mechanisms in the source areas revealed tension cracks and seepage, which reduced the shear strength of the slope, induced the loss of fine particles, and resulted in slope instability. The fallen gravel piled up at the slope toe. Intense rainfall could then swiftly move the deposits to the river mouth and form alluvial fans. The terrain at Houyenshan mainly features well-developed erosion gullies produced by rainfall, surface runoff, and endogenetic processes that make the slope faces uneven.

The results of this study indicate that source areas where landslide occurrence frequencies face high landslide hazard. Rainfall causes the slope toe deposits to become debris flows in the river channel. The Houyenshan tunnel is located below the river mouth, so it is in a high hazard zone, which creates great

concern for road user safety. The zoning and hazard classifications in this study can serve as reference for future plans in pre-disaster remediation, landslide-sensitive area zoning, and river training works.

References

1. Lin J-C, Cheng Y-C, Chia-Horn Jen (2007) Characteristics of the Erosion in Hoyenshan Area, Miaoli. Journal of Chinese Soil Water Conservation 38(3):275–285.(in Chinese)
2. Lin J-C, Chen Y-C, Lin J-W, Jen C-H, Schulte A, Margot Böse (2008) *Experiment on fluvial processes of conglomerate channel-an example of Hoyenshan conglomerate sediments*, Environment and Worlds (17): 21ï½36Department of Geography, National Kaohsiung Normal University). (in Chinese)
3. Jiun-Chuan L (2009) Changes erosion and accumulation characteristics of alluvial fans in Hoyenshan Area. Taiwan Forestry Journal, (in Chinese)
4. Chou H-T, Lee C-F, Huang C-H, Yu-Long Chang (2013) The Monitoring and Flow Dynamics of Gravelly Debris. Journal of Chinese Soil Water Conservation 44(2):144–157 (in Chinese)
5. Chou H-T, Yang H-L, Lee C-F, Chih-Hsuan Huang (2013)). *The Flow Patterns and Geophone Characteristics of Debris Flows at Houyenshan, Miaoli, Taiwan*. Journal of Chinese Soil Water Conservation 46(2):71–78 (in Chinese)
6. Kuang-Tsung Chang Y-H, Chen M-C Cheng (2014) *Study on The Mechanical Behavior of Gravel Formations Using*, Journal of Chinese Soil and Water Conservation. Jour nal of Chinese Soil Water Conservation 45(2):95–102 (in Chinese)
7. Wu Fan-ChiehYJen-Ming, Wong W-M (2005) Study on Micro-Geomorphological Features of Debris Flow on Hillslope of Conglomerate Formation (2005) (in Chinese)
8. Lo C-M, Feng Z-Y, Zhong Y-X, Dong Y-T (2016) Potential Landslide Hazard Zoning based on Numerical Simulation and Hazard Assessment. Journal of Chinese Soil Water Conservation 47(1):1–1 (in Chinese)
9. Crozer MJ (1984) Field assessment of slope instability, In: Slope Instability / ed. by. Brunsen D., Prior D.B. (Editor), New York, John Wiley, Sons Ltd, 103–142
10. Lateltin O, Haemmig C, Raetzo H, Bonnard C (2005) Landslide risk management in Switzerland, Landslides, 2, 313–320

Figures

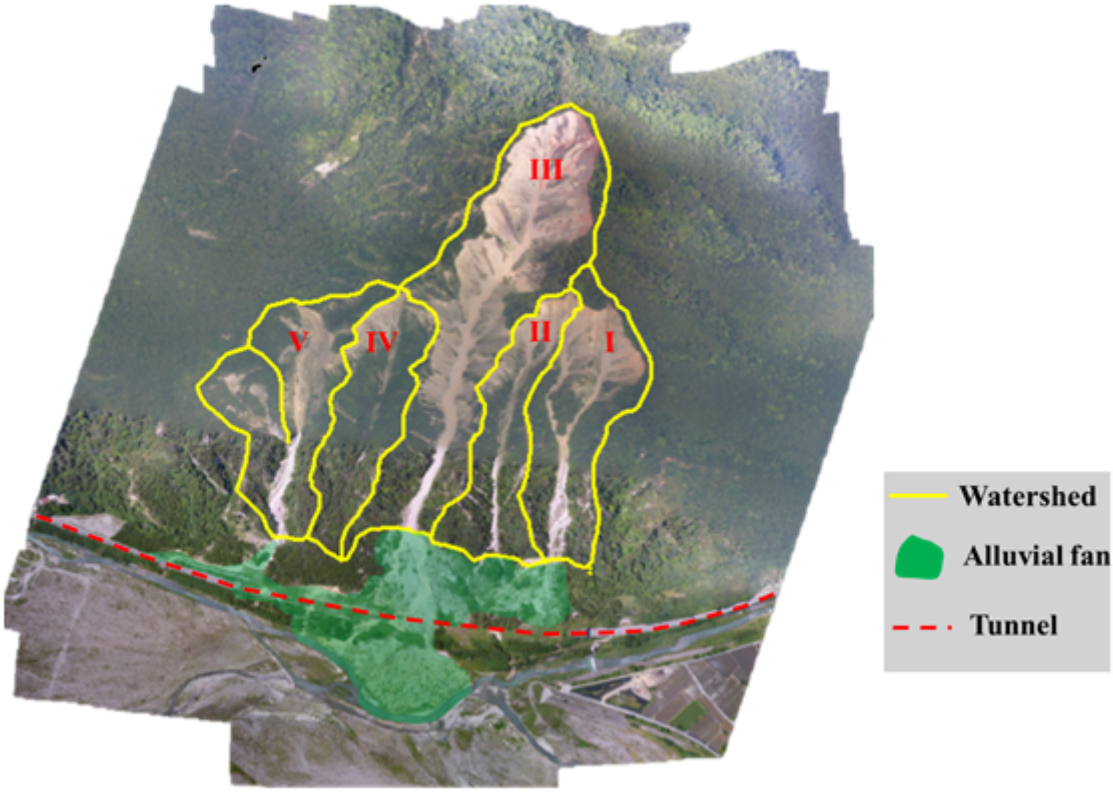

Figure 1

the topographical features of the study area (Houyenshan) Note: The designations employed and the presentation of the material on this map do not imply the expression of any opinion whatsoever on the part of Research Square concerning the legal status of any country, territory, city or area or of its authorities, or concerning the delimitation of its frontiers or boundaries. This map has been provided by the authors.

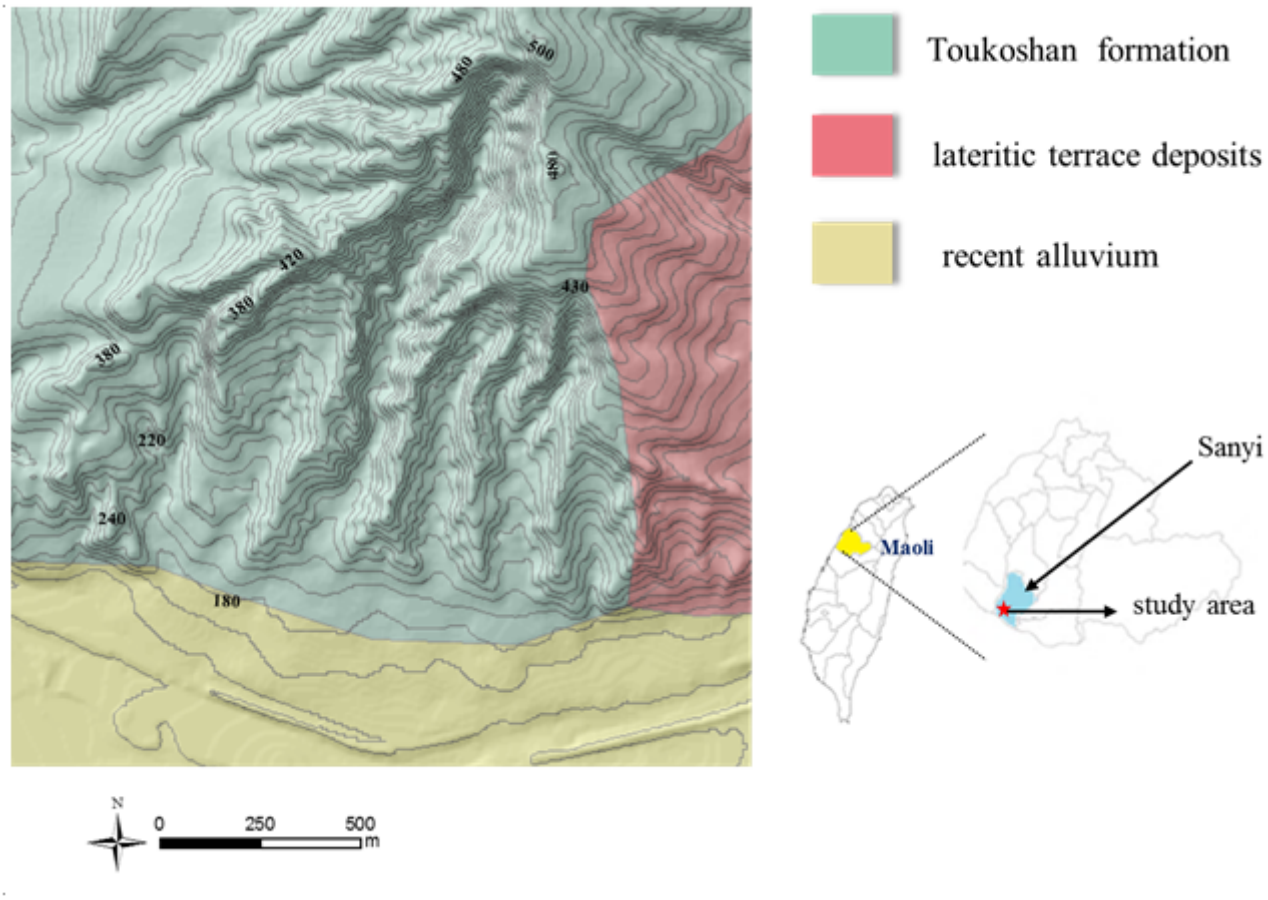

Figure 2

The geological map of the study area Note: The designations employed and the presentation of the material on this map do not imply the expression of any opinion whatsoever on the part of Research Square concerning the legal status of any country, territory, city or area or of its authorities, or concerning the delimitation of its frontiers or boundaries. This map has been provided by the authors.

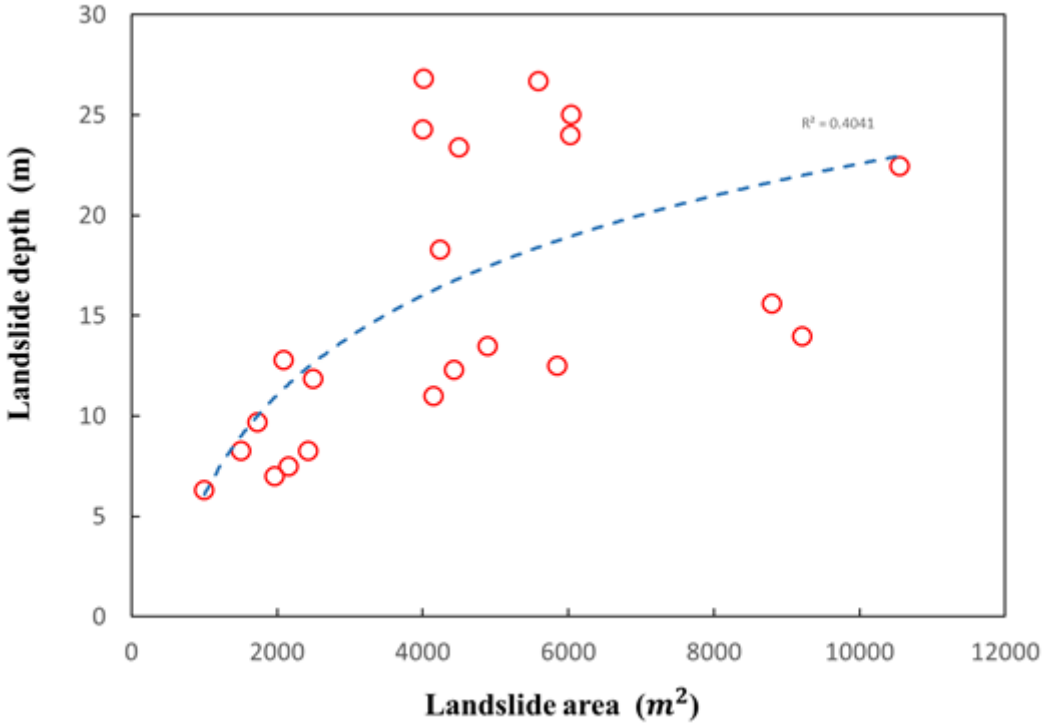

Figure 3

Relationship between landslide area and depth in study area

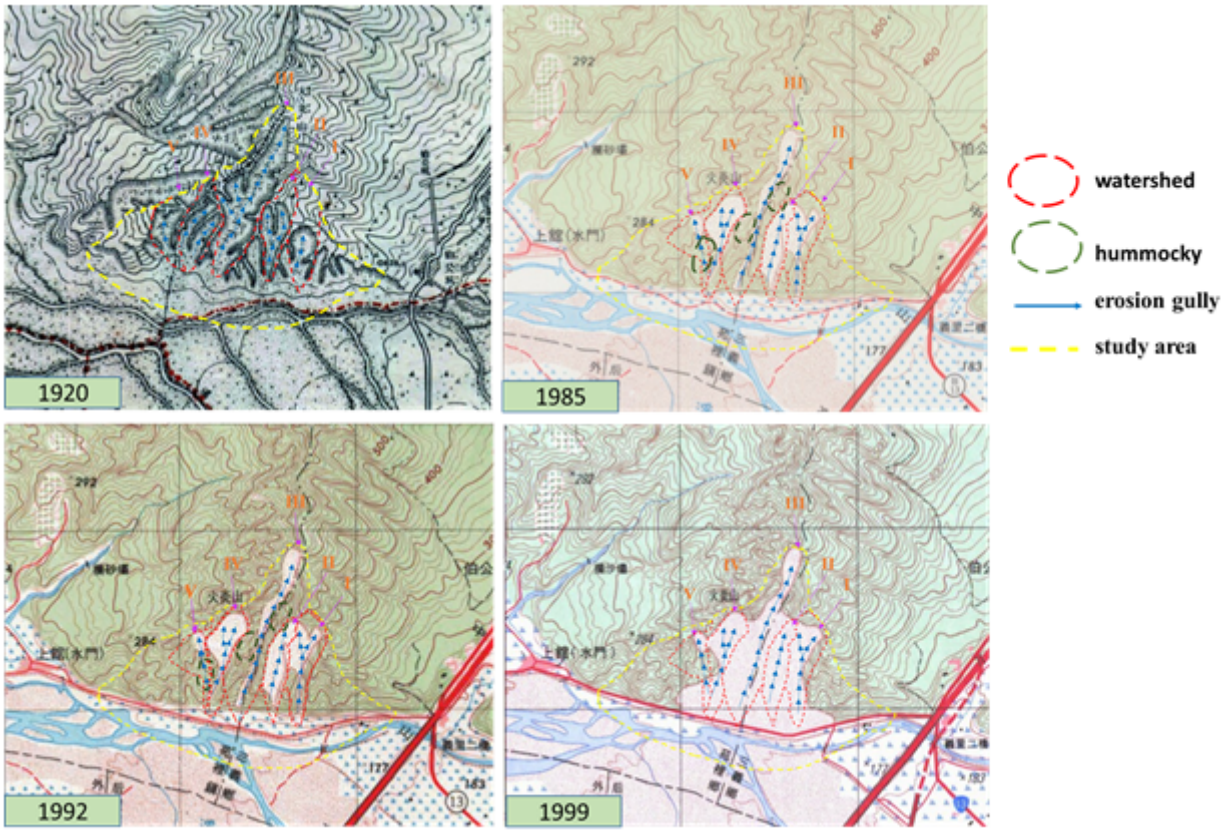

Figure 4

Historical terrain analysis results of study area Note: The designations employed and the presentation of the material on this map do not imply the expression of any opinion whatsoever on the part of Research Square concerning the legal status of any country, territory, city or area or of its authorities, or concerning the delimitation of its frontiers or boundaries. This map has been provided by the authors.

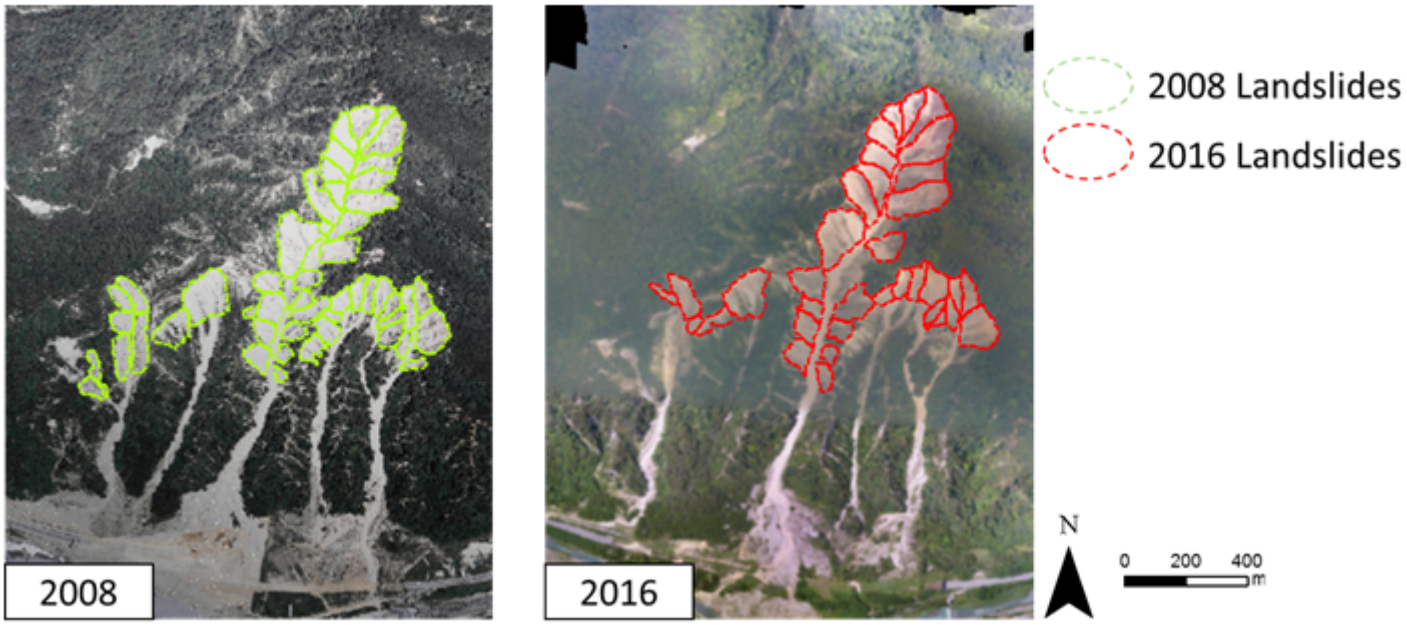

Figure 5

Landslide interpretation results of study area Note: The designations employed and the presentation of the material on this map do not imply the expression of any opinion whatsoever on the part of Research Square concerning the legal status of any country, territory, city or area or of its authorities, or concerning the delimitation of its frontiers or boundaries. This map has been provided by the authors.

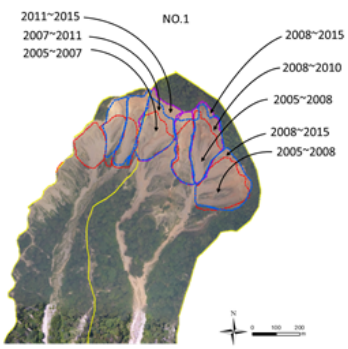

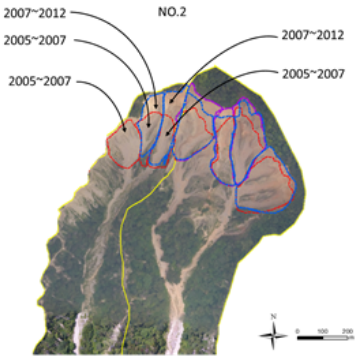

The source area of Pit No. 1 can be divided into three parts, each with a landslide depth of 9 m and continual landslides

The left and right edges of Pit No. 2 touch those of Pits No. 1 and 3, and the most apparent landslide took place in 2012

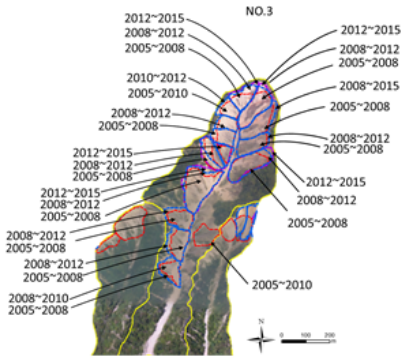

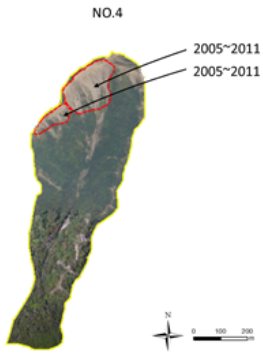

Continual landslides took place in Pit No. 3 within five years, which has the largest area of the five pits; landslide depth exceeded 20 m

Pit No. 4 was relatively more stable than the other four pits with no significant increases in landslide area and historical landslide depth approximately 7 m

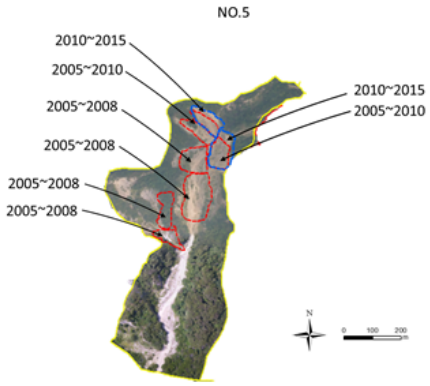

Changes within Pit No. 5 in five years all took place at the source; however, unlike the first few years, landslides only occurred in the source area

Figure 6

Landslide interpretation results of study area (UAV image) Note: The designations employed and the presentation of the material on this map do not imply the expression of any opinion whatsoever on the part of Research Square concerning the legal status of any country, territory, city or area or of its authorities, or concerning the delimitation of its frontiers or boundaries. This map has been provided by the authors.

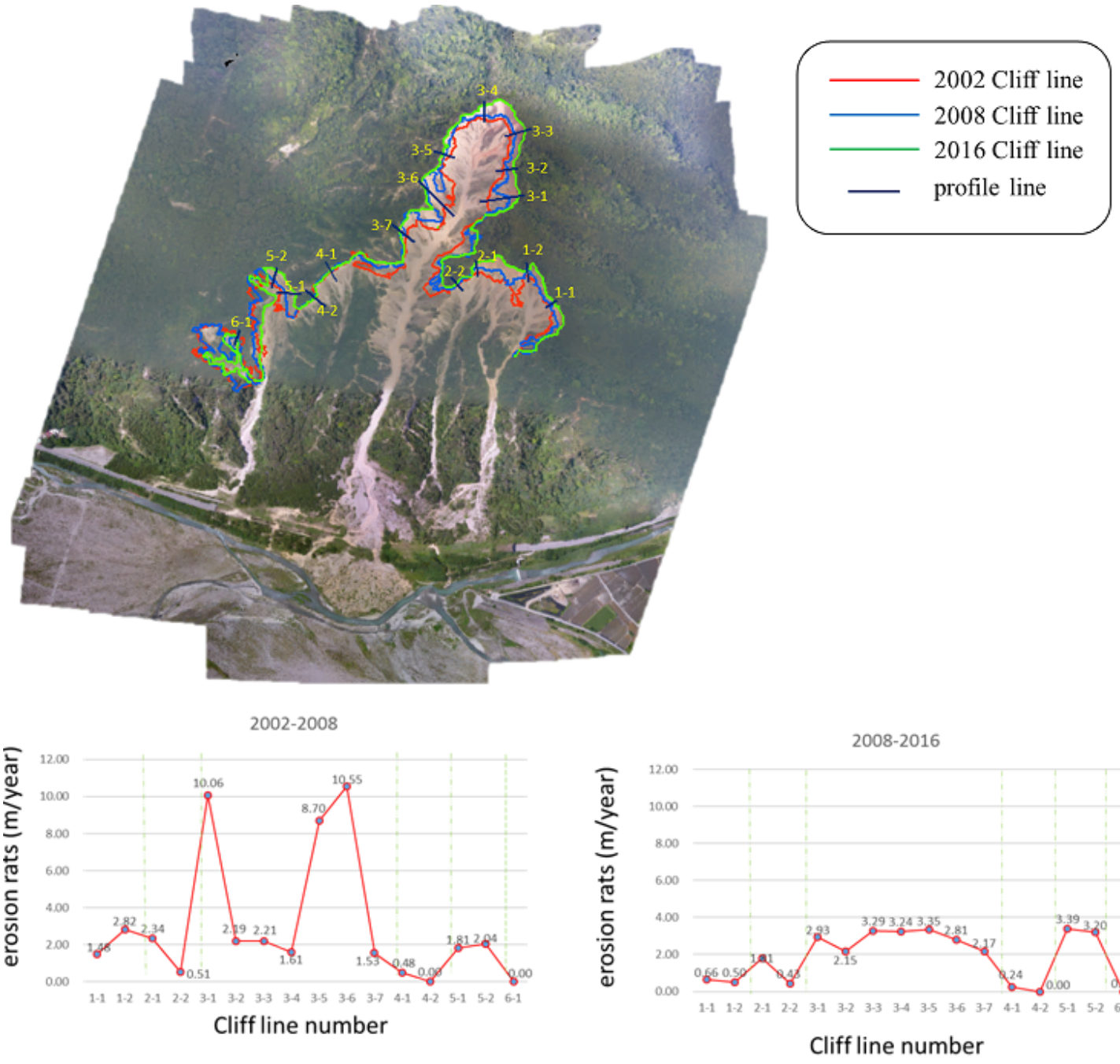

Figure 7

Erosion rates in pits at Houyenshan Note: The designations employed and the presentation of the material on this map do not imply the expression of any opinion whatsoever on the part of Research Square concerning the legal status of any country, territory, city or area or of its authorities, or concerning the delimitation of its frontiers or boundaries. This map has been provided by the authors.

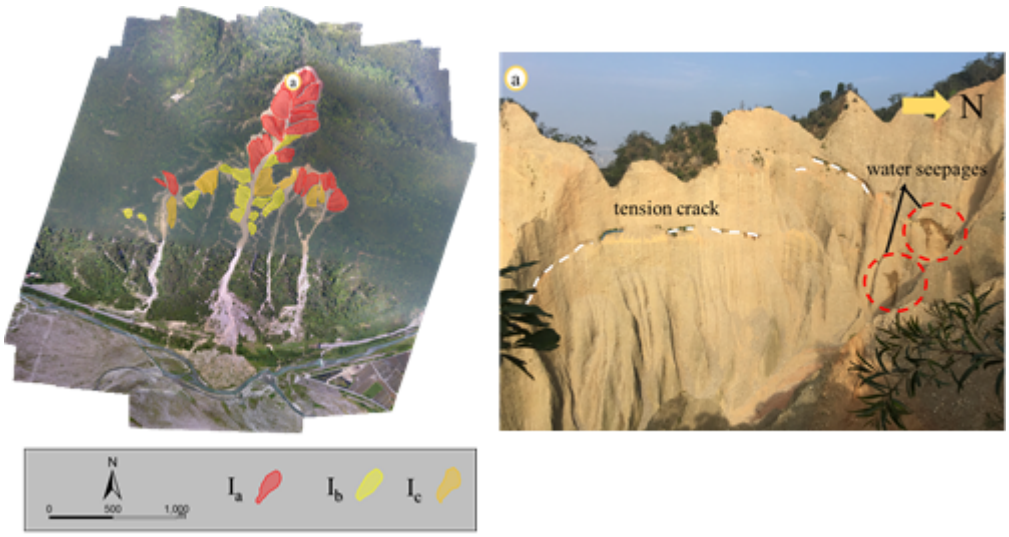

Figure 8

Results of micro-photography interpretation of potential landslide areas and slope stability classification in study area Note: The designations employed and the presentation of the material on this map do not imply the expression of any opinion whatsoever on the part of Research Square concerning the legal status of any country, territory, city or area or of its authorities, or concerning the delimitation of its frontiers or boundaries. This map has been provided by the authors.

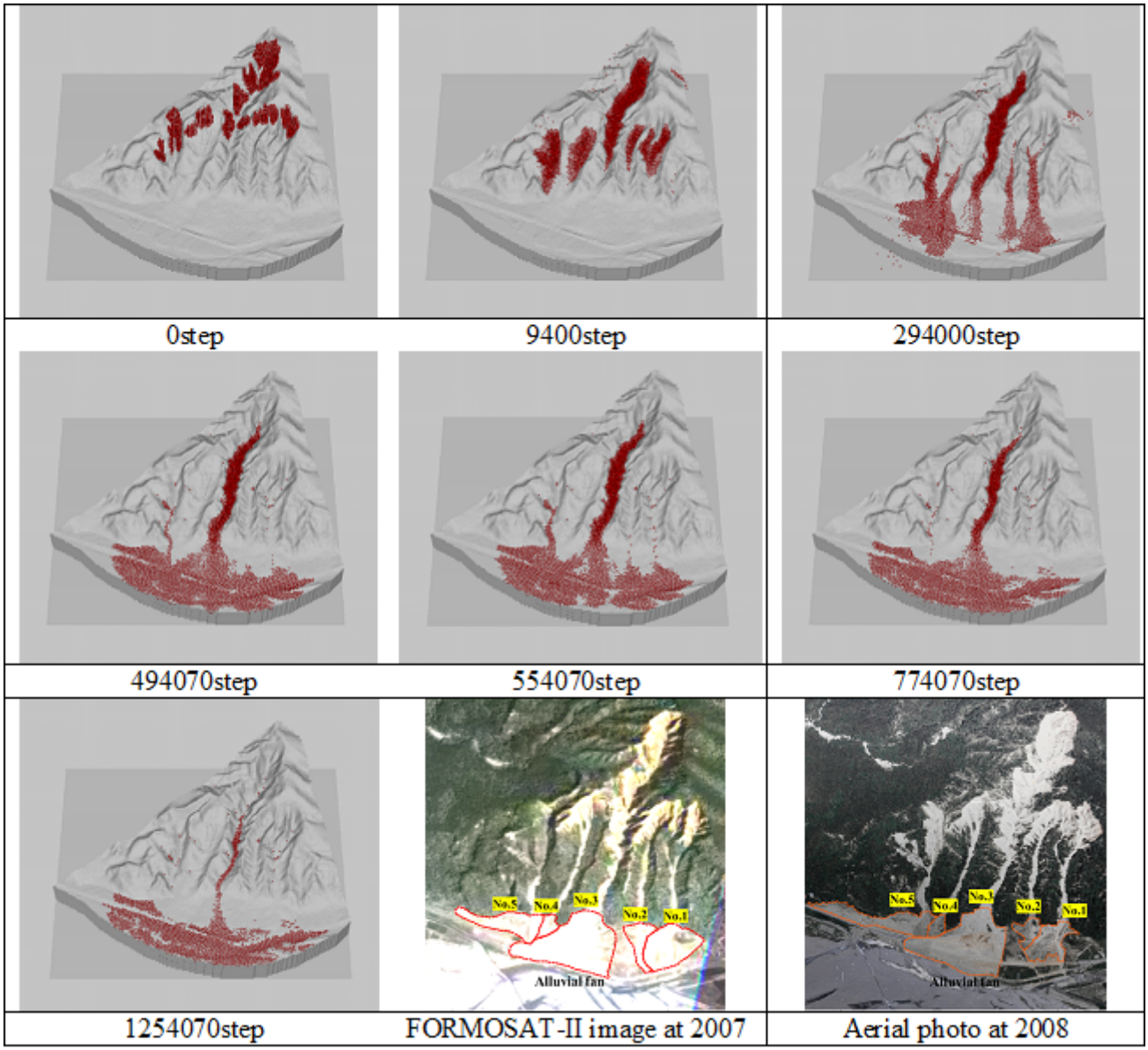

Figure 9

Comparison of historical landslide simulations from 2005 to 2008 in study area Note: The designations employed and the presentation of the material on this map do not imply the expression of any opinion whatsoever on the part of Research Square concerning the legal status of any country, territory, city or area or of its authorities, or concerning the delimitation of its frontiers or boundaries. This map has been provided by the authors.

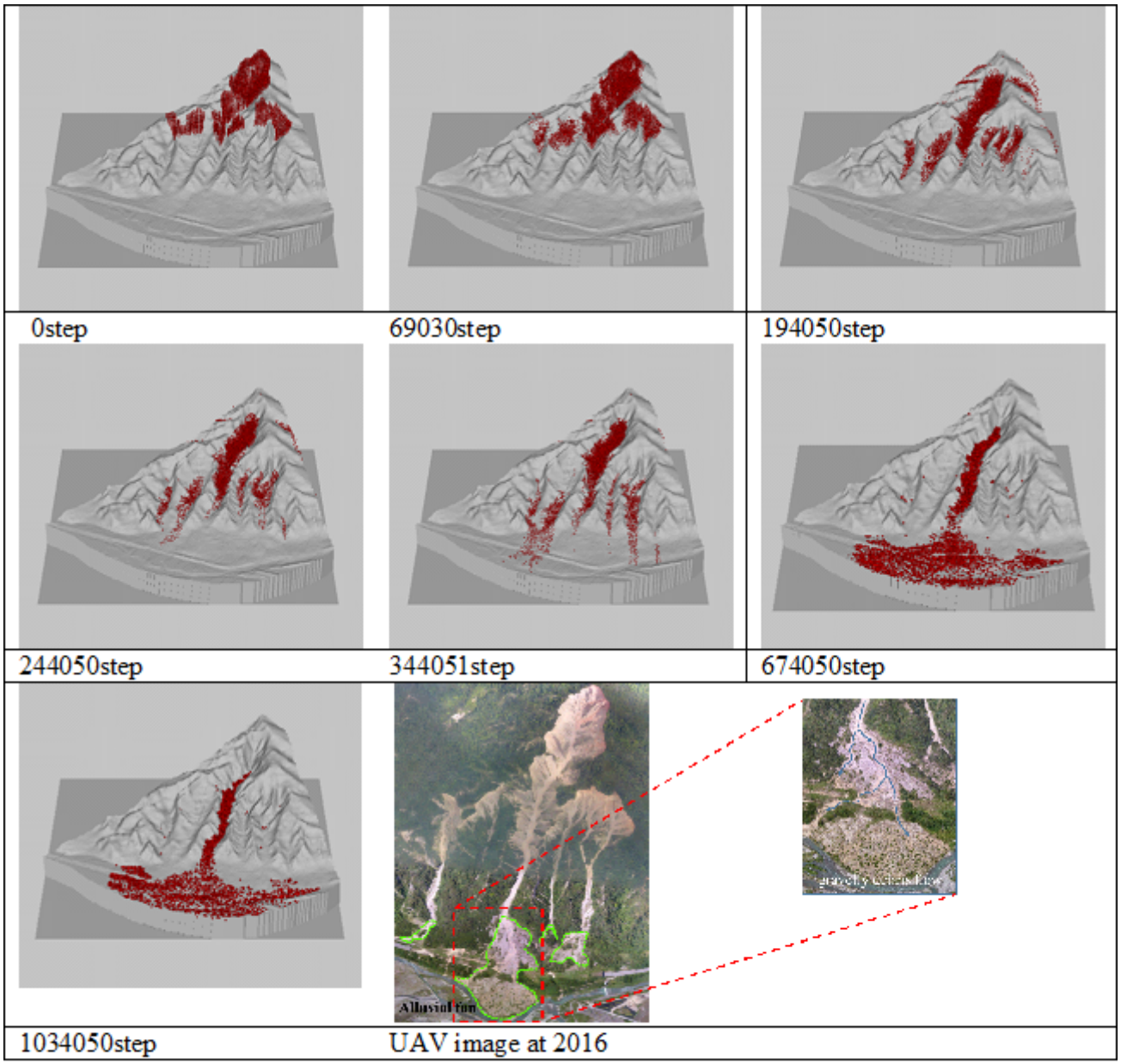

Figure 10

Comparison of historical landslide simulations from 2008 to 2016 in study area Note: The designations employed and the presentation of the material on this map do not imply the expression of any opinion whatsoever on the part of Research Square concerning the legal status of any country, territory, city or area or of its authorities, or concerning the delimitation of its frontiers or boundaries. This map has been provided by the authors.

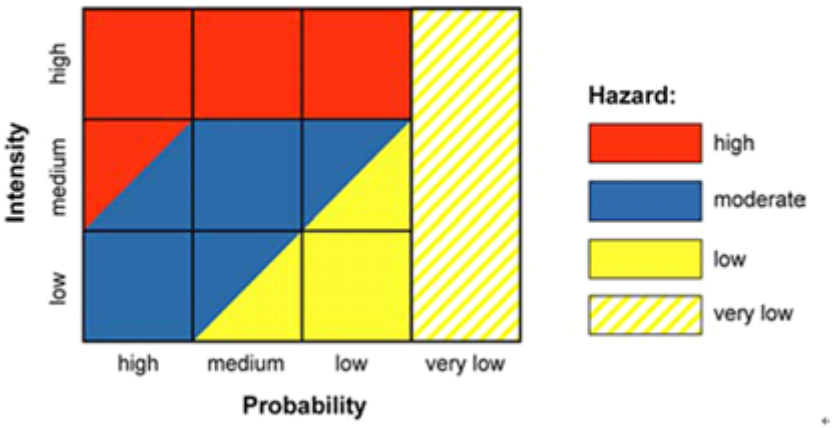

Figure 11

Landslide hazard classification illustration by Switzerland (Lateltin et al, 2005)

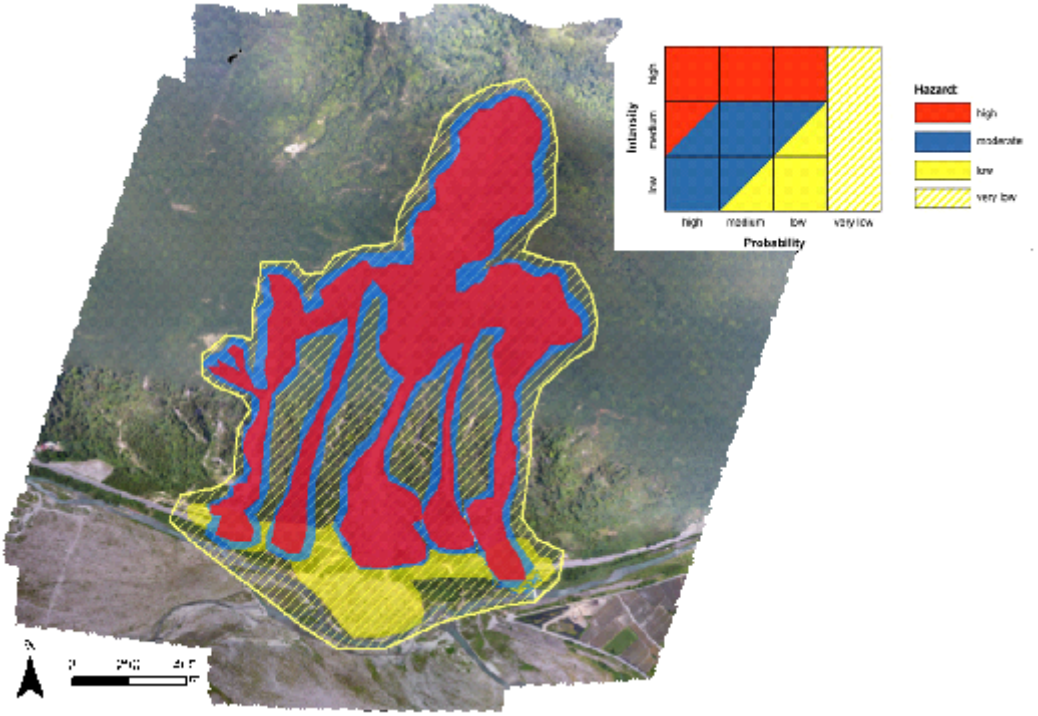

Figure 12

Distribution of potential landslide hazard in study area (base map: UAV orthophoto) Note: The designations employed and the presentation of the material on this map do not imply the expression of any opinion whatsoever on the part of Research Square concerning the legal status of any country, territory, city or area or of its authorities, or concerning the delimitation of its frontiers or boundaries. This map has been provided by the authors.